Adsorption of sodium alginate on calcium carbonate microparticles: Effect of molar mass and composition

R. da Costa, C. Ghobril, P. Perrin, N. Sanson

Adsorption of sodium alginate on calcium carbonate microparticles: Effect of molar mass and composition

R. Da Costa[a, b], C. Ghobril[b], P. Perrin[a,*], N. Sanson[a,*]

[a]Soft Matter Sciences and Engineering, PSL Research University, ESPCI Paris, Sorbonne Université, CNRS UMR 7615, 10 rue Vauquelin, 75231 Paris Cedex 05, France.

[b]L'Oréal Research & Innovation, Avenue Eugène Schueller 1, 93601 Aulnay-sous-Bois, France.

Corresponding author at: Soft Matter Sciences and Engineering, PSL Research University, ESPCI Paris, Sorbonne Université, CNRS UMR 7615, 10 rue Vauquelin, 75231 Paris Cedex 05, France.
E-mail address: nicolas.sanson@espci.fr (N. Sanson) and patrick.perrin@espci.fr (P. Perrin).

Abstract

Sodium alginate and calcium carbonate are natural materials with a high compositional variability. The molar mass and structural composition of sodium alginate and the crystalline structure of calcium carbonate can affect their interactions in pure water. Herein, we studied the adsorption of sodium alginate onto calcium carbonate microparticles in pure water. The adsorption appears to be driven by electrostatic interactions stabilized by calcium ions at the surface of the particles and in solution due to the dissolution of calcium carbonate in pure water. We found that the adsorption of sodium alginate is favored onto microparticles with more calcite. We also found that the adsorption of sodium alginate polymers with low guluronate content (~ 30 %) onto calcium carbonate particles tends to increase for polymers with lower average molar mass and more flexible polymer chains. In contrast, polymers with high guluronate content (~ 65 %) tend to adsorb more onto calcite when they present a lower average molar mass polymers as well as a higher proportion of guluronate monomers.

Keywords: Sodium alginate, Guluronate, Calcium carbonate, Calcite, Vaterite, Adsorption, Chain stiffness, Structural composition

Abbreviations

^{1}H-NMR	Proton nuclear magnetic resonance
Alg_Mw_%G	Sodium alginate_Weight average molar mass_Percentage of Guluronate blocks
Am	Area per monomer of Na-Alg in the adsorbed layer
Ca^{2+}	Calcium ions
$CaCl_2$	Calcium chloride
$CaCO_3$	Calcium carbonate
$CaCO_3$_calcite%	Calcium carbonate_Percentage of calcite vs. vaterite
C_e	Concentration of Polymer at equilibrium
Cf	Concentration of sodium alginate detected in the supernatant by NPOC measurements
Ci	Initial concentration of sodium alginate
Csolid	Concentration of $CaCO_3$
Đ	Dispersity
D_2O-DSS	Deuterium oxide containing 0.05 wt.% of 3-(trimethylsilyl)propionic-2,2,3,3-d4 acid, sodium salt
D_{50}	Average diameter
EDTA	Ethylenediaminetetraacetic acid
Eq.	Equation
ESEM	Environmental scanning electron microscopy
F_G	Molar fraction of guluronate blocks
F_{GG}	Molar fraction of guluronate- guluronate diads
F_{GM}	Molar fraction of guluronate-mannuronate diads
F_M	Molar fraction of mannuronate blocks
F_{MG}	Molar fraction of mannuronate-guluronate diads
F_{MM}	Molar fraction of mannuronate-mannuronate diads
G-blocks	Guluronate blocks
GG-diads	Guluronate-guluronate diads
GM-diads	Guluronate-mannuronate diads
HCl	Hydrochloric acid
K_L	Langmuir constant
M-blocks	Mannuronate blocks
MG-diads	Mannuronate-guluronate diads
MM-diads	Mannuronate-mannuronate diads
M_n	Number average molar mass
M_w	Weight average molar mass
Na_2CO_3	Sodium carbonate
Na-Alg	Sodium alginate
NaCl	Sodium chloride
$NaNO_3$	Sodium nitrate
NPOC	Non-purgeable organic content
S_{BET}	Specific surface area using the Brunauer-Emmett-Teller method
SEC	Size exclusion chromatography
T	Temperature
TGA	Thermogravimetric analysis
TOC	Total organic carbon
XRD	X-ray diffraction
Γ	Amount of adsorbed polymer
Γ_{max}	Maximum amount of adsorbed polymer
η	Illustrative description of the sequence distribution

1. Introduction

Alginates are natural polysaccharides produced by bacteria [1] (*e.g.*, *Azotobacter*) or extracted from brown algae [2] (*e.g.*, *Laminaria hyperborea*) [3–5] consisting of β-D-mannuronate (M-blocks) and α-L-guluronate (G-blocks) that are linked by 1→ 4 bonds. These bonds intercalate between alternating structures of mannuronate-guluronate diads or guluronate-mannuronate diads (MG-diads or GM-diads, respectively). The distribution and ratio of each monomer in the backbone of alginate polymer chains can greatly vary depending on the extraction source of alginate for instance [1–5]. Alginates are known to form gels with strong physical crosslinking bonds in the presence of divalent cations such as calcium ions [6–8]. Grant et al. [9] previously established that guluronate-guluronate diads (GG-diads) are primarily responsible for this phenomenon. These diads are preferentially arranged in a structure called the "egg-box", which selectively interacts with divalent cations. More recently, Donati et al. showed that MG-diads (or GM-diads) junctions can also play a role in the sol-gel transition of alginates [10]. Due to their biocompatibility, biodegradability, and interesting properties in physiological media, sodium alginate (Na-Alg) and calcium alginate gels (Ca-Alg) have been extensively used in the pharmaceutical and food industries [3,8]. One way to form Ca-Alg gels is to release calcium ions following the dissolution of calcium carbonate ($CaCO_3$) under acidic conditions in a solution containing Na-Alg [11,12].

$CaCO_3$ is one of the most abundant materials on Earth [13,14]. This inorganic material is present in limestone [14–17], shells of living marine organisms [16,17], and can also be easily synthesized [16]. Due to its abundance, biocompatibility, and nontoxicity, $CaCO_3$ has been widely investigated in academic research and is used in the food industry as an additive [18] or in the paper industry as a pigment or filler [19,20]. It has three main anhydrous polymorphs: calcite, aragonite, and vaterite [14,16,17]. Calcite is the most thermodynamically stable phase of $CaCO_3$ followed in terms of stability by aragonite and vaterite phases [14,16,17]. The latter two are metastable forms of $CaCO_3$ that can recrystallize as calcite under specific conditions [21,22].

Vaterite, the least thermodynamically stable phase of $CaCO_3$, has been widely studied. The spherical shape of vaterite microparticles, along with their larger pores, makes vaterite a suitable material for biomedical applications, especially for controlled drug delivery [23,24]. $CaCO_3$ can be loaded with a drug of interest through adsorption diffusion and used as a sacrificial template to release the drug in acidic media or by using a chelating agent (*e.g.*, ethylenediaminetetraacetic acid, EDTA, or citric acid) [25–27]. $CaCO_3$ can also be used to

form hollow microcapsules of polymers with defined morphologies [28] using a layer-by-layer technique [25–28]. For instance, Li et al. [29] prepared crosslinked polyacrylamide-alginate spherical hollow microparticles using spherical $CaCO_3$ microparticles as a template to successfully adsorb sodium alginate at the surface of the microparticles in a solution of acrylamide monomers. More recently, Browning et al. [30] showed that Na-Alg chains could adsorb onto the surface of calcite in pure water. The authors concluded that the adsorption was driven by the dissolution of the calcite surface which released calcium ions to promote interactions with Na-Alg. Interestingly, they observed that adsorption was promoted by Na-Alg, which possesses a higher proportion of G-blocks in their backbone. To the best of our knowledge, Browning et al. publication is the only study reported in the literature regarding the adsorption of Na-Alg onto $CaCO_3$ in pure water.

While the adsorption of Na-Alg onto $CaCO_3$ in pure water could depend on the proportion of G-blocks in the Na-Alg backbone, it could also be influenced by various compositional factors given the substantial variability inherent to Na-Alg and to $CaCO_3$ microparticles. In this study, we thus aim at identifying the factors controlling the adsorption of Na-Alg onto $CaCO_3$ surfaces, namely the proportion of each $CaCO_3$ phase, the average molar mass of Na-Alg and the distribution of GG-diads in their backbone.

2. Experimental part

2.1. Materials

Calcium carbonate microparticles (quoted $CaCO_3$_calcite% in this study to reflect their calcite composition compared to vaterite) were either purchased from Sigma-Aldrich® ($CaCO_3$_100%), provided by L'Oréal Research ($CaCO_3$_38%), or synthesized as described in the literature [27] ($CaCO_3$_38%, $CaCO_3$_22%, and $CaCO_3$_3%). Sodium carbonate (Na_2CO_3) and calcium chloride ($CaCl_2$), used for the synthesis of $CaCO_3$ were purchased from Sigma-Aldrich®. Sodium alginate samples (quoted Alg_M_w_%G in this study based on their weight average molar mass, M_w, and the percentage of G-blocks in their backbone) were kindly provided by DuPont™ and were used as received. Hydrochloric acid (HCl), sodium nitrate ($NaNO_3$), sodium chloride (NaCl), and deuterium oxide containing 0.05 wt %) 3-(trimethylsilyl)propionic-2,2,3,3-d4 acid and sodium salt (D_2O-DSS) were purchased from Sigma-Aldrich®. Ethylenediaminetetraacetic acid (EDTA) was purchased from VWR

Chemicals®. Ultra-pure water (resistivity = 18 MΩcm) obtained from a Milli-Q® water purification system was used to prepare the solutions.

2.2. Methods

2.2.1. $CaCO_3$ microparticles synthesis

Spherical $CaCO_3$ microparticles were synthesized according to a previously reported method [27]. Briefly, an equal volume of aqueous solutions of 0.33 mol.L^{-1} calcium chloride ($CaCl_2$) and 0.33 mol.L^{-1} sodium carbonate (Na_2CO_3) were added in this order into a round-bottom-flask and mechanically stirred for 30 min at 25 °C. The precipitate was filtered using a 1.2 µm Whatman filter (GF/C grade), rinsed several times with water and dried at 72 °C overnight. Several syntheses were conducted under the same conditions and exhibited good reproducibility for the formation of $CaCO_3$_3%. $CaCO_3$_22% microparticles were synthesized using the same protocol, but in a total volume of 5 L (vs. 400 mL), filtration issues during the post-treatment led to the development of more calcite microparticles. The filtration step was slower and less efficient than that for smaller-scale synthesis. Therefore, the reaction time was increased as well as the proportion of water in the filtrate prior drying. These two events most likely led to the recrystallization of part of the synthesized vaterite microparticles into more stable calcite particles [21].

2.2.2. Characterization of $CaCO_3$ microparticles

The average size (D_{50}) of the $CaCO_3$ microparticles was determined after gold metallization using a Quattro Environmental Scanning Electron Microscope (ESEM, ThermoFisher©) and in water using a Mastersizer 3000 (Malvern Panalytical©). The specific surface area (S_{BET}) of the $CaCO_3$ microparticles was characterized by nitrogen adsorption–desorption isotherms using the Brunauer-Emmett-Teller (BET) method, performed using Tristar II plus (Micrometrics™). Samples with lower surface areas were characterized using krypton adsorption-desorption isotherms instead of nitrogen and were conducted on a Belsorp-Max II (MicrotracBEL Corp). The crystal structure was determined by X-ray diffraction (XRD) using a Philips X' Pert diffractometer. The results were compared with existing databases and Rietveld refinement was used to determine the proportion of each $CaCO_3$ phase in the sample.

2.2.3. Characterization of Na-Alg

The ratio of G-blocks and M-blocks in each Na-Alg sample was reported by the supplier as a percentage range and was further characterized using a consistent method described in the literature by Grasdalen et al. [31–34]. Briefly, Na-Alg was mildly hydrolyzed under acidic conditions at 100 °C (pH 3) for 30 to 105 min. Hydrolyzed Na-Alg (25 mg) were dissolved in D_2O-DSS (1 mL) with EDTA (7.5 mg) and analyzed using proton nuclear magnetic resonance spectroscopy (^{1}H-NMR) performed on a Bruker Neo 400 operating at 400.22 MHz equipped with an ATMA ^{1}H-BBI probe of 5 mm heated at 80 °C. The number and weight average molar masses (M_n and M_w, respectively) as well as the dispersity ($Đ = M_w/M_n$) were determined by size exclusion chromatography (SEC) on a Malvern Viscotek TDA 302 system equipped with a triple detector with three OH-pak SB-806M HQ columns in series. The mobile phase was an aqueous solution at 0.2 M $NaNO_3$, and with a flow rate of 0.7 $mL.min^{-1}$. The calibration curve was based on poly(ethylene oxide) standards from Malvern. The residual water content was characterized by thermogravimetric analysis (TGA) using a Q600 SDT (TA Instruments).

2.2.4. Adsorption isotherms

Adsorption isotherms were obtained using a depletion method. Aqueous Na-Alg solutions with an initial concentration of 1 $g.L^{-1}$ were prepared and stirred for 24 h prior to analysis. Dry $CaCO_3$ microparticles (0.5 g) were introduced into centrifuge tubes with a 50 mL capacity. Specific volumes of water and Na-Alg aqueous solution were then introduced in this order to reach the desired Na-Alg concentration ranging from 0 to 800 $mg.L^{-1}$ in a total volume of 15 mL. The blank solution contained only water. Preliminary experiments performed at different equilibrium times showed no change in Na-Alg concentration in the supernatant after 2 h, relative to 24 h. The samples were left to equilibrate on a tube rotator for 4 h. The dispersions were subsequently centrifuged once at 6000 g for 30 min and again for 15 min after removing and transferring the supernatant into a new centrifuge tube. The Non-Purgeable Organic Carbon (NPOC) content of the supernatant was measured using a calibrated TOC-L analyzer (Shimadzu). During the measurements, the solutions were automatically acidified to 10 wt % with a 2 $mol.L^{-1}$ solution of HCl and purged with nitrogen to remove traces of inorganic carbonates. The value obtained for the blank solution was first subtracted from that obtained for the suspension supernatant to characterize the residual concentration of Na-Alg. Replicate NPOC measurements based on two to three sample

injections were performed for each blank, suspension, and calibration solution. Each adsorption isotherm was replicated at least twice.

The amount of adsorbed polymer, Γ, expressed in $mg.m^{-2}$, was calculated using the following equation:

$$\Gamma = \frac{C_0 - C_f}{S_{BET} C_{solid}} \quad \text{Eq. 1}$$

Where C_0 is the concentration of Na-Alg initially introduced to the sample ($mg.L^{-1}$), C_f is the concentration of Na-Alg detected by NPOC measurements in the supernatant ($mg.L^{-1}$), and S_{BET} is the specific surface area of $CaCO_3$ ($m^2.mg^{-1}$), and C_{solid} is the concentration of $CaCO_3$ microparticles ($mg.L^{-1}$).

2.2.5. Zeta potential of CaCO3 microparticles with adsorbed Na-Alg

$CaCO_3$ microparticles remaining in the centrifuge pellets after the removal of the supernatant were dispersed in an aqueous solution of sodium chloride at 10^{-3} $mol.L^{-1}$. Zeta potential measurements were conducted using a Zetasizer Nano series (Malvern Panalytical).

3. Results and Discussion

Na-Alg aqueous solutions containing dispersed $CaCO_3$ microparticles exhibit a pH of 10. At this pH, $CaCO_3$ microparticles and Na-Alg polymer chains are negatively charged [35,36]. This raises questions regarding the nature of the interaction between Na-Alg and $CaCO_3$ in pure water. In the present study we aim at investigating the key parameters that control such interaction. $CaCO_3$ microparticles with various crystalline phase compositions and Na-Alg with different average molar masses and structural compositions were selected and thoroughly characterized.

The characteristics of $CaCO_3$ microparticles, such as their size, calcite/vaterite composition, and specific surface area are summarized in Table 1. As shown in Fig. 1, $CaCO_3$ microparticles with an increased proportion of calcite phase exhibit more rhombohedra-shaped microparticles [14,16,17].

Table 1: Characteristics of calcium carbonate ($CaCO_3$) microparticles.

$CaCO_3$	% Calcite (vs. vaterite)	D_{50} (µm)	S_{BET} ($m^2.g^{-1}$)
$CaCO_3$_3%	3	6 ± 1	8.1

$CaCO_3$_22%	22	10 ± 2	4.7
$CaCO_3$_38%	38	7 ± 2	2.4
$CaCO_3$_100%	100	20 ± 5	0.6

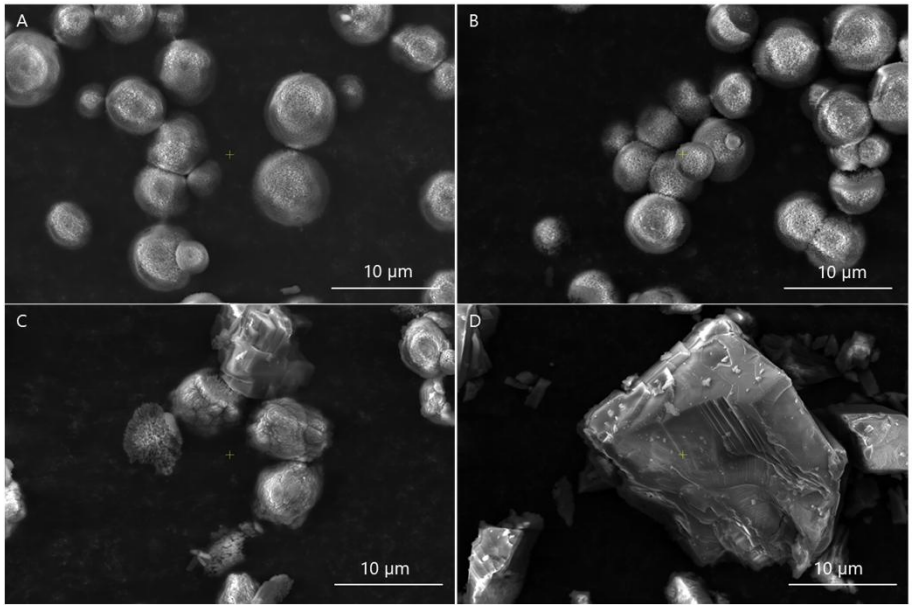

Fig. 1: Scanning electron microscopy (SEM) micrographs of the calcium carbonate microparticles studied ($CaCO_3$_calcite%). A) $CaCO_3$_3%; B) $CaCO_3$_22%; C) $CaCO_3$_38% and D) $CaCO_3$_100%.

The characteristics of Na-Alg polysaccharides, such as their average molar mass and monomer composition, are listed in Table 2. All polysaccharides contained 9-15 wt % residual water.

The composition of Na-Alg samples was characterized by ^{1}H-NMR following mild hydrolysis of the polymer and using a consistent method developed by Grasdalen et al. [31–34]. Three specific ^{1}H-NMR signals were identified: the first signal (I, 5.1-5.2 ppm) was attributed to the anomeric hydrogen of guluronic acid in G-blocks, and the second signal (II, 4.7-4.9 ppm) to both the overlap of the anomeric hydrogen of mannuronic acid in M-blocks and the fifth hydrogen of alternating MG-diads. Finally, the third signal (III, 4.5-4.6 ppm) was attributed to the fifth hydrogen of guluronic acid in G-blocks. The area below each signal was then used in equations determined by Grasdalen et al. [31–34] (Eq. 2) to calculate the molar fractions of guluronate and mannuronate blocks (F_G and F_M, respectively) and the molar fractions of GG-diads, MG-diads, GM-diads and mannuronate-mannuronate diads (MM-diads) (F_{GG}, F_{MG}, F_{GM} and F_{MM}, respectively). A parameter η, defined as an illustrative way of characterizing the sequence distribution, was also determined with $0 \leq \eta < 1$ for an abundance of homopolymeric M-blocks and G-blocks, $\eta = 1$ for a random sequence, and $1 < \eta \leq 2$ for an abundance of alternating MG-diads and GM-diads.

$$F_G = \frac{I}{II + III} \quad F_M = 1 - F_G$$

$$F_{GG} = \frac{III}{II + III}, \; F_{MG} = F_{GM} = F_G - F_{GG} \quad \text{and} \quad F_{MM} = F_M - F_{MG} \qquad \text{Eq. 2}$$

$$\eta = \frac{F_{MG}}{F_M F_G}$$

The composition of each Na-Alg is in good agreement with the range provided by the supplier (see Fig. S2 in the supplementary information for all ^{1}H-NMR spectra). Based on these results, a hypothetical repartition of each monomer along the backbone of a single Na-Alg chain was established as shown in Fig. 2. These results highlight the great variability in the composition of natural polysaccharides, providing an opportunity to explore how it affects the adsorption of Na-Alg onto $CaCO_3$ microparticles.

Table 2: Characteristics of sodium alginate (Na-Alg) samples.

		SEC			^{1}H-NMR					
Na-Alg	% G	M_w (kg.mol^{-1})	M_n (kg.mol^{-1})	Đ	F_G	F_M	F_{GG}	F_{MG} F_{GM}	F_{MM}	η
Alg_39k_G65	65	39	21	1.9	0.61	0.39	0.54	0.07	0.32	0.31
Alg_168k_G65	65	168	112	1.5	0.57	0.43	0.50	0.08	0.34	0.31
Alg_140k_G30	30	140	76	1.8	0.27	0.73	0.12	0.15	0.58	0.74
Alg_222k_G30	30	222	121	1.8	0.32	0.68	0.21	0.11	0.57	0.49
Alg_309k_G30	30	309	190	1.6	0.33	0.67	0.18	0.14	0.54	0.64
Alg_306k_G45	45	306	143	2.1	0.47	0.53	0.30	0.17	0.36	0.66

Fig. 2: Hypothetical distribution of G-blocks (G spheres) and M-blocks (M squares) along the backbone of Na-Alg chains.

3.1. Influence of the crystalline structure of CaCO3 microparticles

The impact of the crystal phase composition of $CaCO_3$ microparticles on the adsorption of Na-Alg was first investigated. Adsorption isotherms were carried out with Alg_309k_G30 in pure water and $CaCO_3$ microparticles of varying calcite and vaterite compositions (equilibrium pH of the dispersion around 10). As depicted in Fig. 3A, all adsorption isotherms exhibit the same behavior that is characteristic of a Langmuir adsorption. The amount of adsorbed Na-Alg, Γ, increases with polymer concentration with initial slopes ranging from 2-20 $mL.m^{-2}$. This increase is followed by an adsorption plateau at high polymer concentrations (maximum amount of adsorbed polymer, Γ_{max}) [37,38]. All the experimental adsorption isotherms were fitted to the Langmuir equation (Eq. 3). Experimental values of Γ_{max} as well as the Langmuir constant determined from the model are reported in Table 3. Values obtained from the fitted model are reported in the supporting information in Table S1.

$$\Gamma = \frac{\Gamma_{max} K_L C_e}{1 + K_L C_e} \qquad \text{Eq. 3}$$

Where Γ is the amount of adsorbed polymer ($mg.m^{-2}$), Γ_{max} is the maximum amount of adsorbed polymer ($mg.m^{-2}$), K_L is the Langmuir constant related to the binding-strength coefficient characteristic of the affinity of the polymer for the solid surface ($L.mg^{-1}$) and C_e is the equilibrium concentration of polymer in solution ($mg.L^{-1}$).

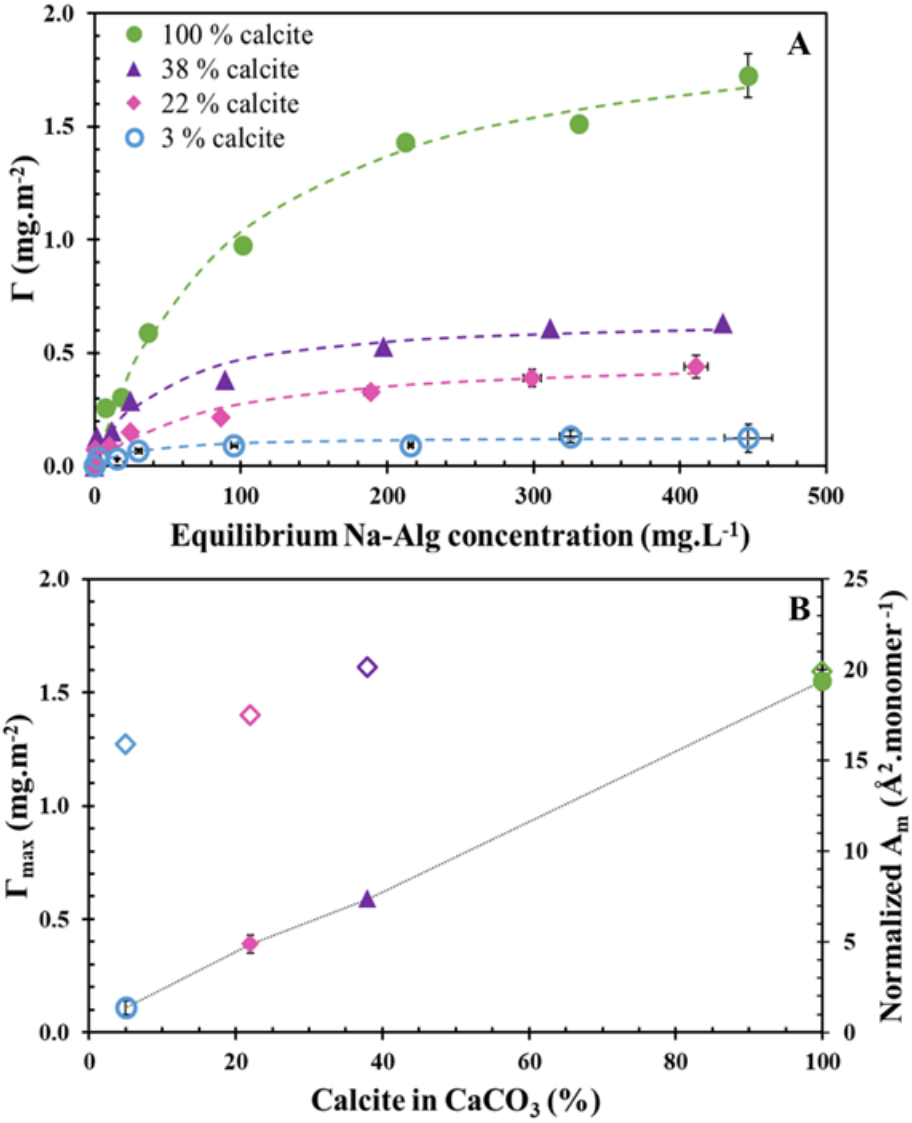
A
100 % calcite
38 % calcite
22 % calcite
3 % calcite
Γ (mg.m-2)
Equilibrium Na-Alg concentration (mg.L-1)
B
Γmax (mg.m-2)
Normalized Am (Å2.monomer-1)
Calcite in CaCO3 (%)

Fig. 3: Influence of the calcite content (vs. vaterite) of $CaCO_3$ microparticles on the adsorption of Na-Alg. A) Adsorption isotherms of Alg_309k_G30 at 25 °C onto $CaCO_3$ microparticles. The amount of adsorbed Na-Alg, Γ, was represented as a function of the equilibrium concentration of Na-Alg. The dashed lines represent the theoretical Langmuir adsorption model fit. B) The maximum amount of Na-Alg adsorbed in $mg.m^{-2}$, Γ_{max}, is the average Γ value at the plateau of each experimental isotherm (the shape of the symbols is the same as that used in the isotherms). The dotted line is a guide for the eye. When the error bars are not visible, they are within the symbol. The area per monomer normalized by the percentage of calcite (Normalized A_m) in $Å^2.monomer^{-1}$ was calculated from the Γ_{max} values and is represented as a function of the percentage of the calcite composition in $CaCO_3$ microparticles (empty lozenges).

Table 3: Adsorption data of Alg_309k_G30 onto $CaCO_3$ microparticles with various calcite contents.

		Experimental data			***Langmuir equation***
Na-Alg	$CaCO_3$	Γ_{max} ($mg.m^{-2}$)	A_m ($Å^2.monomer^{-1}$)	Normalized A_m ($Å^2.monomer^{-1}$)	K_L ($L.mg^{-1}$)
Alg_309k_G30	$CaCO_3$_100%	1.60 ± 0.10	20	20	0.010
	$CaCO_3$_38%	0.60 ± 0.09	53	20	0.025
	$CaCO_3$_22%	0.40 ± 0.07	79	17	0.013
	$CaCO_3$_3%	0.10 ± 0.06	318	16	0.035

The theoretical adsorption model of Langmuir fits greatly the experimental dataset (Fig. 3A and Table S1). Hence, Na-Alg is likely to be adsorbed at the surface of $CaCO_3$ microparticles as a monolayer reaching full surface coverage. The initial slopes of the different isotherms suggest a favorable interaction between adsorbate and adsorbent with a medium affinity, which is in good agreement with K_L values obtained from the Langmuir adsorption model [39,40].

In pure water at pH 10, Na-Alg polymer chains and $CaCO_3$ microparticles are both negatively charged [35,36]. However, it has been reported that in addition to carbonate ions (CO_3^{2-}), calcium ions (Ca^{2+}) are also present on the surface of $CaCO_3$ microparticles [36]. These divalent cations exhibit a strong affinity for carboxylate groups and thus promote the adsorption of negatively charged polymer chains onto the surface of $CaCO_3$ microparticles by ion binding. This was also reported by Browning et al. as a driving force for the adsorption of Na-Alg onto calcite microparticles [30] and by Arumughan et al. for the adsorption of weak polyelectrolytes, such as carboxymethylcellulose, onto like-charged surfaces [41]. This observation provides a possible explanation for the similarity in K_L values among the different experiments.

Ca^{2+} ions can increase the adsorption of polyelectrolytes onto the surface of like-charged solids [42]. In water, $CaCO_3$ microparticles dissolve and release Ca^{2+} and CO_3^{2-} ions until reaching an equilibrium (Eq. 4).

$$CaCO_{3(s)} \leftrightarrows Ca^{2+}_{(aq)} + CO_3^{2-}{}_{(aq)} \quad \text{Eq. 4}$$

Since vaterite is slightly more soluble than calcite in water, one could assume that Na-Alg would adsorb more at its surface. Interestingly, our experiments show the opposite. The maximum amount of Na-Alg adsorbed at the surface of $CaCO_3$ microparticles, Γ_{max}, increases with the calcite content (Table 3, Fig. 3A and Fig. 3B). At equilibrium in water, a 15 ± 5 mg.L^{-1} concentration of Ca^{2+} ions is detected for $CaCO_3$ microparticles regardless of the crystalline phase within a few minutes [43,44]. Therefore, in our experiments the ionic strength of the dispersions is buffered at 1.5 ± 0.3 mmol.L^{-1}. Consequently, the increase of Γ_{max} values with the calcite content cannot be explained by the presence of calcium ions in solution. In the light of our results, we come to the conclusion that Na-Alg only adsorbs onto the calcite phase of the $CaCO_3$ microparticles. We hypothesize that this arises from the specific attributes of the calcite phase in terms of surface ion availability, as compared to vaterite. Furthermore, the shape of the microparticles could also play a role in creating a distinct interface for the adsorption of Na-Alg.

In an effort to probe the conformation adopted by Na-Alg at the surface of $CaCO_3$ microparticles, we determined the area per monomer of Na-Alg in the adsorbed layer using Eq. 5 assuming a monolayer adsorption. This value was also scaled by the calcite content of the microparticles (Normalized A_m). Our findings are summarized in Fig. 3 and in Table 3.

$$A_m = \frac{S_{tot\ CaCO_3}}{NaAlg\ monomers} = \frac{M_0}{\Gamma_{max} N_a} \quad \text{Eq. 5}$$

Where A_m is the area per monomer and the area per monomer normalized by the calcite composition in $CaCO_3$ microparticles (Å^2.monomer $^{-1}$) respectively, $S_{tot\ CaCO_3}$ is the total surface of $CaCO_3$ (Å^2), Na-Alg molecule is the number of monomers of Na-Alg present in the adsorbed layer, M_0 is the average molar mass of a Na-Alg monomer (M_0 ~ 191 g.mol^{-1} assuming a value of 0.7 for the ionization degree of Na-Alg in pure water) and Γ_{max} is the maximum amount of adsorbed Na-Alg (g.Å^{-2}).

The size of a Na-Alg repeat unit is on average equal to 5 Å [45,46]. Hence, whether considering a sphere with a diameter of 5 Å or a cube with sides measuring 5 Å, it can be

inferred that the minimum area occupied by a Na-Alg monomer should be approximately 20-25 Å². Interestingly, once scaled by the proportion of calcite, the value of A_m is on average equal to 18 ± 2 $Å^2$.monomer $^{-1}$ (Table 3). This value is also close to the average surface area per calcium ions of calcite (20.8 $Å^2$) [46]. Therefore, assuming that Na-Alg adsorbs as a monolayer at the surface of calcite two conceivable conformation emerge. The polymer can either adsorb flat onto $CaCO_3$, wherein each adsorption site accommodates a Na-Alg monomer (Fig. 4A) or adopt a more extended conformation by forming loops, tails, and trains at the solid surface. In the latter, the number of monomers not directly bound to the solid surface (dark green circles) is the same as the number of particle free adsorption sites (unoccupied grey squares)(Fig. 4B).

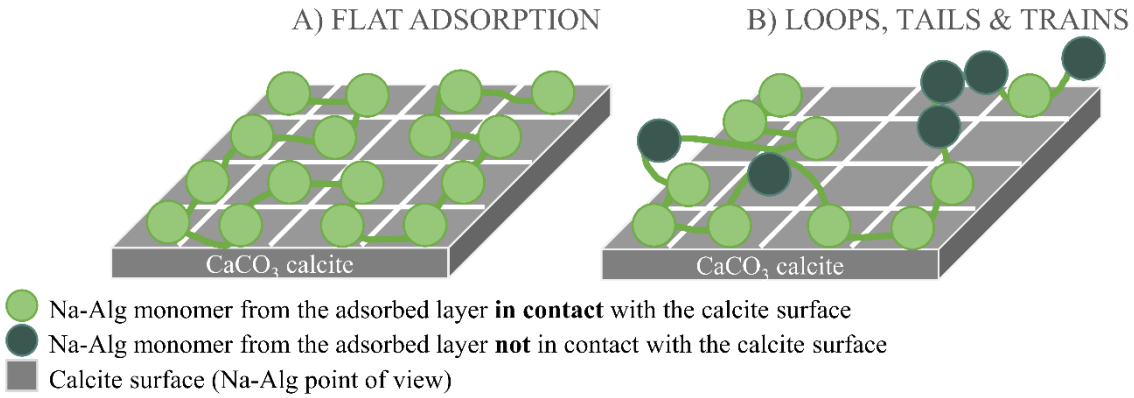

Fig. 4: Schematic representation of the possible conformation of the Na-Alg adsorbed layer at the surface of calcite $CaCO_3$ microparticles in pure water where the average area per monomer is 20 $Å^2$.monomer $^{-1}$. Calcite was represented as a plane surface due to the size difference between the solid and the polymer. A) Flat adsorption of the polymer: all monomers in the adsorbed layer of Na-Alg bind to the surface and B) Loops, tails and trains formation: a proportion of monomers present in the adsorbed layer are not in direct contact with the calcite surface but the number of monomers that do not bind with the surface (dark green circles) is close to the number of free adsorption sites (grey squares).

Polyelectrolytes are more likely to adsorb in a flat conformation when interacting strongly with a surface [48]. While our K_L values suggest a favorable interaction between the polymer and the surface, they are not characteristic of a strong interaction. We then believe that the second scenario is more likely to occur. Additionally, weak polyelectrolytes such as

Na-Alg are prone to form loops and tails at low charge densities as would be expected for alginate interacting with Ca^{2+} ions in pure water [30,48,49].

Zeta potential measurements provide insights regarding the adsorption of Na-Alg onto $CaCO_3$ microparticles. Upon dispersing $CaCO_3$ microparticles in salt-free aqueous solutions of Na-Alg for four hours, the zeta potential of both $CaCO_3$_100% and $CaCO_3$_38% microparticles decreased from -8 to -40 mV (Fig. S3).

Through this experiment we have shown that the Na-Alg adsorption in pure water depends on the crystalline phase of $CaCO_3$ microparticles. As a matter of fact, a better adsorption of alginates is observed on particles with higher calcite content. This phenomenon is likely to be driven by an electrostatic interaction due to the presence of Ca^{2+} ions at the surface of the particles. In the following sections, we discuss the impact of Na-Alg composition on its adsorption onto $CaCO_3$ microparticles in pure water.

3.1.1. Influence of Na-Alg composition

In a recent study, Browning et al. [30] showed that the adsorption of Na-Alg onto calcite depends on the proportion of G-blocks in the backbone of the polysaccharide. Herein, we aim at investigating the effect of the average molar mass and distribution of the different M and G monomers of the alginates on their adsorption onto $CaCO_3$ microparticles in an aqueous medium. To achieve this, we conducted experiments using Na-Alg samples with comparable proportions of G-blocks (~ 30 %). Γ_{max} values are plotted as a function of the average molar mass and the F_{GG} of Na-Alg in Fig. 5. They are determined from the experimental dataset given in Fig. S4A and Fig. S4B where full isotherms are presented. All informative values are summarized in Table 4.

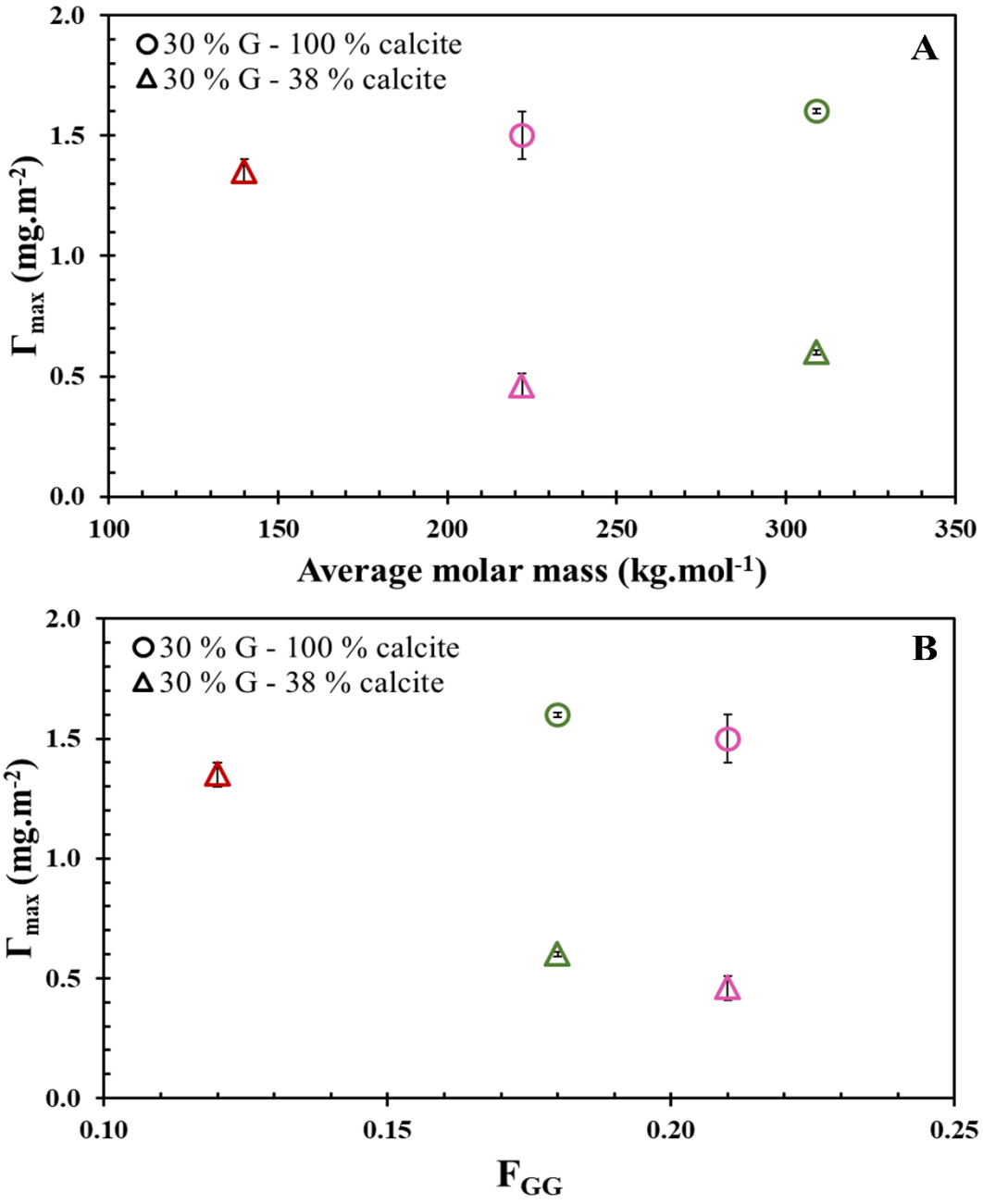

Fig. 5: Γ_{max} in pure water of Na-Alg with 30 % G-blocks on $CaCO_3$ particles (38 % and 100 % calcite) as a function of : A) the Na-Alg average molar mass. B) the proportion of GG-diads (F_{GG}) along the backbone.

Table 4: Adsorption data of several Na-Alg with 30 % G-blocks and various average molar masses adsorbed onto $CaCO_3$ microparticles.

		Experimental data			*Langmuir equation*
$CaCO_3$	Na-Alg	Γ_{max} ($mg.m^{-2}$)	A_m ($Å^2.monomer^{-1}$)	Normalized A_m ($Å^2.monomer^{-1}$)	K_L ($L.mg^{-1}$)
$CaCO_3$_100%	Alg_309k_G30	1.6 ± 0.1	20	20	0.010
	Alg_222k_G30	1.5 ± 0.2	21	21	0.002
	Alg_140k_G30	N/A			
$CaCO_3$_38%	Alg_309k_G30	0.60 ± 0.09	53	20	0.025
	Alg_222k_G30	0.46 ± 0.07	69	26	0.006
	Alg_140k_G30	1.4 ± 0.2	23	9	0.011

As previously shown in Fig. 3 and Table 3, Γ_{max} values of a single Na-Alg onto $CaCO_3$ microparticles increase with the calcite content. When considering the same $CaCO_3$ microparticle, it is apparent that the adsorption of Na-Alg with the same proportion of G-blocks is significantly increased for Alg_140k_G30 compared to the two other polymers (Table 4 and Fig. 5). Regarding the adsorption of this polymer onto $CaCO_3$_100%, the absence of an adsorption plateau suggests that the system is out of equilibrium (see Fig. S4A). The increase in average molar mass between Alg_222k_G30 and Alg_309_G30 does not appear to have a substantial impact on the maximum amount of adsorbed polymer. It was previously reported that an increase in the average molar mass of the polymer is likely to result in an increase of the Γ_{max} values. In our case this trend is not evident. The distribution of each monomer and diad along the polymer backbone could potentially account for this deviation (Table 2 and Fig. 2). Indeed, the proportion of GG-diads can impact the interaction of the polymer with Ca^{2+} at the surface of $CaCO_3$ microparticles or in solution. Additionally, due to their structure, G-blocks are stiffer than linear M-blocks [10,30]. Hence two Na-Alg with the same F_G can differ due to their average molar mass as well as their proportion of diads F_{GG} in their backbone, which can increase the rigidity of the polymer chains. As shown in Fig. 5B, Γ_{max} decreases as F_{GG} increases and thus as the rigidity of the polymer chains increases. This is in good agreement with previously reported Monte Carlo simulations on the adsorption of weak polyelectrolytes onto oppositely charged surfaces [50–52]. We assume that flexible polymer chains allow to bring closer G-blocks from a single Na-Alg polymer chain or from multiple Na-Alg polymer chains to complex Ca^{2+} ions thus promoting the polymer adsorption onto the surface of the $CaCO_3$ microparticles.

Conversely, for Na-Alg with 65 % of G-blocks, the adsorption onto the surface of $CaCO_3$ microparticles increases for the most locally rigid polymer, Alg_39k_G65 (Table 5). However, in both Na-Alg, most G-blocks are already in a preferential conformation to interact with Ca^{2+} ions (high F_{GG}, Table 2 and Fig. 2). For Na-Alg with high guluronate content, we can reasonably assume that the adsorption is promoted by the lower average molar mass as well as the slightly higher proportion of G-blocks for Alg_39k_G65 compared to Alg_168k_G65 (0.61 vs 0.57). It is worth noting that the Γ_{max} values for $CaCO_3$_100% and Na-Alg with 65 % G-blocks are in the tenth of milligram per square meter range (Table 5). The values for a monolayer coverage are usually closer to one to two milligrams per square meter [50]. The high Γ_{max} values obtained with these polymers could be due to interactions between the adsorbed layer of Na-Alg and free polymer chains that are not bound to the surface (inter-chain interactions). This phenomenon could also occur during the adsorption of Alg_140k_G30 onto $CaCO_3$_100% as no plateau is reached, which is inconsistent with Langmuir's theory of adsorption (Fig. S4A).

Consequently, it appears that for Na-Alg with a low proportion of G-blocks, both the average molar mass and the proportion of GG-diads and hence, the stiffness of the polymer chain impact their adsorption onto $CaCO_3$ microparticles in water. However, for Na-Alg with a high proportion of G-blocks, thus composed essentially of homopolymeric regions, multiple GG-diads are in a preferential conformation to complex Ca^{2+} ions. Therefore, we assume that the proportion of G-blocks will have a stronger impact on their adsorption onto the surface of $CaCO_3$ microparticles in water.

Table 5: Adsorption data of several Na-Alg with 65 % G-blocks and various average molar masses (39K and 168K) adsorbed onto $CaCO_3$ microparticles (38% and 100% calcite).

		Experimental data			***Langmuir equation***
$CaCO_3$	Na-Alg	Γ_{max} ($mg.m^{-2}$)	A_m ($Å^2.monomer^{-1}$)	Normalized A_m ($Å^2.monomer^{-1}$)	K_L ($L.mg^{-1}$)
$CaCO_3$_100%	Alg_168k_G65	9.3 ± 2.0	3	3	0.010
	Alg_39k_G65	11.5 ± 1.0	3	3	0.015
$CaCO_3$_38%	Alg_168k_G65	0.9 ± 0.4	35	13	0.027
	Alg_39k_G65	1.6 ± 0.5	20	8	0.035

As previously, we determined the normalized A_m of the adsorbed layer for all adsorption experiments (Table 4 and Table 5). Similar to Alg_309k_G30, A_m values determined for Alg_222k_G30 are close to 20 $Å^2$.monomer^{-1} and the two conformation previously proposed in Fig. 4 can thus again apply. However, some of the calculated A_m values fall significantly below 20 $Å^2$. monomer^{-1}, suggesting that the surface available for the polymer is insufficient to accommodate a Na-Alg monomer. Hence, the polymer chain conformation is probably more extended in a direction perpendicular to the particle surface, resulting in the formation of loops, tails and trains (Fig. 6).

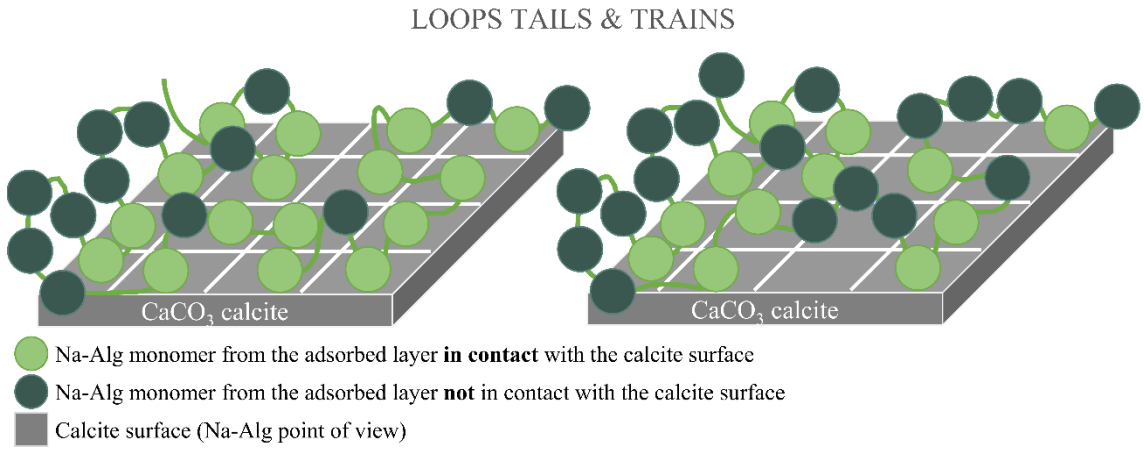

Fig. 6: Schematic representation of the possible conformation of the Na-Alg adsorbed layer at the surface of calcite $CaCO_3$ microparticles in pure water when the area per monomer is below 20 $Å^2$.monomer $^{-1}$. In both representations there is more Na-Alg monomers in the monolayer than adsorption sites on calcite particles. On the left all adsorption sites are occupied by a Na-Alg monomer while on the right they are not. Calcite is represented as a plane surface due to the size difference between the solid and the polymer.

3.1.2. Influence of G-block proportion

Herein, we focus on the impact of the proportion of G-blocks in the backbone of Na-Alg by performing adsorption isotherms with 300 kg.mol^{-1} Na-Alg (see Fig. S5 for full isotherms). All informative values are summarized in Table 6.

Table 6: Adsorption data of two Na-Alg with an average molar mass close to 300 kg.mol^{-1} and various G-blocks adsorbed onto $CaCO_3$ microparticles (38% and 100% calcite).

		Experimental data			*Langmuir equation*
$CaCO_3$	Na-Alg	Γ_{max} (mg.m^{-2})	A_m (Å^2.monomer^{-1})	Normalized A_m (Å^2.monomer^{-1})	K_L (L.mg^{-1})
$CaCO_3$_100%	Alg_306k_G45	0.90 ± 0.1	35	35	0.034
	Alg_309k_G30	1.60 ± 0.1	20	20	0.010
$CaCO_3$_38%	Alg_306k_G45	0.57 ± 0.1	56	21	0.030
	Alg_309k_G30	0.60 ± 0.1	53	20	0.025

Consistent with the previous results, Γ_{max} values determined for the adsorption of the same Na-Alg onto $CaCO_3$ microparticles increases with the calcite content. Interestingly, Γ_{max} slightly increases for Alg_309k_G30, which has less G-blocks (F_G = 0.33 vs. 0.47) and GG-diads (F_{GG} = 0.18 vs. 0.30) along its backbone. As it was observed for Na-Alg with a low G-blocks proportion, the rigidity of the polymer chain has a stronger impact than the proportion of G-blocks.

4. Conclusion and perspectives

This work aims at probing the adsorption in water of sodium alginate onto the surface of calcium carbonate microparticles by varying their average molar mass as well as the composition and distribution of the M and G-blocks. The interaction between the two materials arises from an electrostatic interaction driven by the presence of calcium ions at the surface of calcium carbonate microparticles, which interact with the guluronate residues of sodium alginate in water. We showed that sodium alginate adsorbs better onto calcium carbonate microparticles with a higher calcite content for reasons that require further investigations. Focusing on sodium alginate, we show that the polymer-solid interaction is strongly dependent on the distribution of guluronate and mannuronate residues in the sodium alginate backbone. Adsorption increases for low guluronate content polymers as the local stiffness of the polymer chains decreases (more mannuronate diads). For high guluronate content, adsorption increases with the proportion of guluronate blocks. We explain our findings by the ability of the more flexible polymer chains to adopt an extended conformation instead of a flat one, resulting in the formation of loops, tails and trains and by more favorable interactions between guluronate residues and calcium ions. To complement our study and gain a deeper understanding of this intricate interaction, the modeling of calcium carbonate

polymorph surfaces could provide insights into the increased affinity of sodium alginate for the calcite phase. Additionally, confirming the conformation adopted by sodium alginate chains upon adsorption onto the surfaces of calcium carbonate microparticles could provide further clarification about this phenomenon. In conclusion, to limit the influence of the average molar mass, we may also adjust the proportion of each repeating unit along Na-Alg backbone of same length. Indeed, we could employ a C5-epimerase to catalyze the conversion of mannuronate into guluronate monomers to sweep the M/G ratio [30,41,53–55].

CRediT authorship contribution statement

Raquel Da Costa: Conceptualization, Methodology, Software, Investigation, Writing - original draft, Visualization. **Nicolas Sanson:** Conceptualization, Methodology, Investigation, Writing - review & editing. **Patrick Perrin:** Conceptualization, Methodology, Investigation, Writing - review & editing. **Cynthia Ghobril:** Investigation, Writing - review & editing, Supervision, Funding acquisition.

Declaration of competing interest

This work has been supported by L'Oréal Research and Innovation funding for the Ph.D. of Raquel Da Costa.

Acknowledgments

This work has also been supported by funding from the Association Nationale de la Recherche et de la Technologie (ANRT) for the CIFRE PhD (2019/1625). The authors thank DuPont™ for providing all the sodium alginate samples. The authors also thank Mohamed Hanafi from the Soft Matter Sciences and Engineering laboratory for the conduction of the SEC experiments, Priscilla Riva from L'Oréal Advanced Research for the conduction of ^{1}H-NMR spectroscopy, Institute of Porous Materials of Paris (IMAP) and especially Mathilde Renouard at ESPCI Paris, for the use and conduction of the experiments using the Tristar II High Throughput Surface Area and Porosity Analyzer plus Micrometrics, Institute Chemistry Biology Innovation (CBI) at ESPCI Paris, for the use of their particle size analyzer Mastersizer 3000, Laboratoire Interdisciplinaire des Environnements Continentaux (LIEC) at Université de Lorraine and especially Angelina Razafitianamaharavo, for low surface area analysis by Krypton adsorption at 77 K.

References

[1] P.A.J. Gorin, J.F.T. Spencer, Exocellular alginic acid from azotobacter vinelandii, Can. J. Chem. 44 (1966) 993–998. https://doi.org/10.1139/v66-147.

[2] T.J. Painter, 4 - Algal Polysaccharides, in: G.O. Aspinall (Ed.), The Polysaccharides, Academic Press, 1983: pp. 195–285. https://doi.org/10.1016/B978-0-12-065602-8.50009-1.

[3] W.R. Gombotz, S. Wee, Protein release from alginate matrices, Advanced Drug Delivery Reviews. 31 (1998) 267–285. https://doi.org/10.1016/S0169-409X(97)00124-5.

[4] K.Y. Lee, D.J. Mooney, Alginate: Properties and biomedical applications, Progress in Polymer Science. 37 (2012) 106–126. https://doi.org/10.1016/j.progpolymsci.2011.06.003.

[5] Z. Belattmania, S. Kaidi, S. El Atouani, C. Katif, F. Bentiss, C. Jama, A. Reani, B. Sabour, V. Vasconcelos, Isolation and FTIR-ATR and 1H NMR Characterization of Alginates from the Main Alginophyte Species of the Atlantic Coast of Morocco, Molecules. 25 (2020) 4335. https://doi.org/10.3390/molecules25184335.

[6] I. Braccini, S. Pérez, Molecular Basis of Ca2+-Induced Gelation in Alginates and Pectins: The Egg-Box Model Revisited, Biomacromolecules. 2 (2001) 1089–1096. https://doi.org/10.1021/bm010008g.

[7] T. Baumberger, O. Ronsin, From thermally activated to viscosity controlled fracture of biopolymer hydrogels, J. Chem. Phys. 130 (2009) 061102. https://doi.org/10.1063/1.3078267.

[8] L. Rolland, E. Santanach-Carreras, T. Delmas, J. Bibette, N. Bremond, Physicochemical properties of aqueous core hydrogel capsules, Soft Matter. 10 (2014) 9668–9674. https://doi.org/10.1039/C4SM02012J.

[9] G.T. Grant, E.R. Morris, D.A. Rees, P.J.C. Smith, D. Thom, Biological interactions between polysaccharides and divalent cations: The egg-box model, FEBS Letters. 32 (1973) 195–198. https://doi.org/10.1016/0014-5793(73)80770-7.

[10] I. Donati, S. Holtan, Y.A. Mørch, M. Borgogna, M. Dentini, New Hypothesis on the Role of Alternating Sequences in Calcium−Alginate Gels, Biomacromolecules. 6 (2005) 1031–1040. https://doi.org/10.1021/bm049306e.

[11] K.I. Draget, K. Østgaard, O. Smidsrød, Alginate-based solid media for plant tissue culture, Appl Microbiol Biotechnol. 31 (1989) 79–83. https://doi.org/10.1007/BF00252532.

[12] L.W. Chan, H.Y. Lee, P.W.S. Heng, Production of alginate microspheres by internal gelation using an emulsification method, International Journal of Pharmaceutics. 242 (2002) 259–262. https://doi.org/10.1016/S0378-5173(02)00170-9.

[13] K.Y. Chong, C.H. Chia, S. Zakaria, M.S. Sajab, Vaterite calcium carbonate for the adsorption of Congo red from aqueous solutions, Journal of Environmental Chemical Engineering. 2 (2014) 2156–2161. https://doi.org/10.1016/j.jece.2014.09.017.

[14] L.M.M. Costa, G.M. de Olyveira, R. Salomão, Precipitated calcium carbonate nano-microparticles: applications in drug delivery, Adv Tissue Eng Regen Med Open Access. 3 (2017) 336–340. https://doi.org/10.15406/atroa.2017.03.00059.

[15] C.G. Kontoyannis, N.V. Vagenas, Calcium carbonate phase analysis using XRD and FT-Raman spectroscopy, Analyst. 125 (2000) 251–255. https://doi.org/10.1039/A908609I.

[16] Y. Boyjoo, V.K. Pareek, J. Liu, Synthesis of micro and nano-sized calcium carbonate particles and their applications, J. Mater. Chem. A. 2 (2014) 14270–14288. https://doi.org/10.1039/C4TA02070G.

[17] F. Liendo, M. Arduino, F.A. Deorsola, S. Bensaid, Factors controlling and influencing polymorphism, morphology and size of calcium carbonate synthesized through the carbonation route: A review, Powder Technology. 398 (2022) 117050. https://doi.org/10.1016/j.powtec.2021.117050.

[18] P. Chaiwanon, P. Puwastien, A. Nitithamyong, P.P. Sirichakwal, Calcium Fortification in Soybean Milk and In Vitro Bioavailability, Journal of Food Composition and Analysis. 13 (2000) 319–327. https://doi.org/10.1006/jfca.1999.0854.

[19] R. Eriksson, J. Merta, J.B. Rosenholm, The calcite/water interface: I. Surface charge in indifferent electrolyte media and the influence of low-molecular-weight polyelectrolyte, Journal of Colloid and Interface Science. 313 (2007) 184–193. https://doi.org/10.1016/j.jcis.2007.04.034.

[20] A. Barhoum, H. Rahier, R.E. Abou-Zaied, M. Rehan, T. Dufour, G. Hill, A. Dufresne, Effect of Cationic and Anionic Surfactants on the Application of Calcium Carbonate Nanoparticles in Paper Coating, ACS Appl. Mater. Interfaces. 6 (2014) 2734–2744. https://doi.org/10.1021/am405278j.

[21] O. Cherkas, T. Beuvier, F. Zontone, Y. Chushkin, L. Demoulin, A. Rousseau, A. Gibaud, On the kinetics of phase transformations of dried porous vaterite particles immersed in deionized and tap water, Advanced Powder Technology. 29 (2018) 2872–2880. https://doi.org/10.1016/j.apt.2018.08.008.

[22] K. Simkiss, Variations in the Crystalline Form of Calcium Carbonate precipitated from Artificial Sea Water, Nature. 201 (1964) 492–493. https://doi.org/10.1038/201492a0.

[23] Y.I. Svenskaya, H. Fattah, O.A. Inozemtseva, A.G. Ivanova, S.N. Shtykov, D.A. Gorin, B.V. Parakhonskiy, Key Parameters for Size- and Shape-Controlled Synthesis of Vaterite Particles, Crystal Growth & Design. 18 (2018) 331–337. https://doi.org/10.1021/acs.cgd.7b01328.

[24] D.B. Trushina, T.V. Bukreeva, M.V. Kovalchuk, M.N. Antipina, CaCO3 vaterite microparticles for biomedical and personal care applications, Materials Science and Engineering: C. 45 (2014) 644–658. https://doi.org/10.1016/j.msec.2014.04.050.

[25] N. Sudareva, H. Popova, N. Saprykina, S. Bronnikov, Structural optimization of calcium carbonate cores as templates for protein encapsulation, J Microencapsul. 31 (2014) 333–343. https://doi.org/10.3109/02652048.2013.858788.

[26] G.B. Sukhorukov, D.V. Volodkin, A.M. Günther, A.I. Petrov, D.B. Shenoy, H. Möhwald, Porous calcium carbonate microparticles as templates for encapsulation of bioactive compounds, J. Mater. Chem. 14 (2004) 2073–2081. https://doi.org/10.1039/B402617A.

[27] D.V. Volodkin, N.I. Larionova, G.B. Sukhorukov, Protein Encapsulation via Porous CaCO3 Microparticles Templating, Biomacromolecules. 5 (2004) 1962–1972. https://doi.org/10.1021/bm049669e.

[28] A. Yashchenok, B. Parakhonskiy, S. Donatan, D. Kohler, A. Skirtach, H. Möhwald, Polyelectrolyte multilayer microcapsules templated on spherical, elliptical and square calcium carbonate particles, J. Mater. Chem. B. 1 (2013) 1223. https://doi.org/10.1039/c2tb00416j.

[29] Y.-L. Li, M.-L. Zhu, X.-Y. Li, X.-H. Li, Y. Jiang, A highly expandable and tough polyacrylamide – alginate microcapsule, RSC Adv. 6 (2016) 44896–44901. https://doi.org/10.1039/C6RA05711J.

[30] K.L. Browning, I.N. Stocker, P. Gutfreund, S.M. Clarke, The effect of alginate composition on adsorption to calcium carbonate surfaces, Journal of Colloid and Interface Science. 581 (2021) 682–689. https://doi.org/10.1016/j.jcis.2020.07.088.

[31] H. Grasdalen, B. Larsen, O. Smidsrød, A p.m.r. study of the composition and sequence of uronate residues in alginates, Carbohydrate Research. 68 (1979) 23–31. https://doi.org/10.1016/S0008-6215(00)84051-3.

[32] H. Grasdalen, B. Larsen, O. Smisrod, 13C-n.m.r. studies of monomeric composition and sequence in alginate, Carbohydrate Research. 89 (1981) 179–191. https://doi.org/10.1016/S0008-6215(00)85243-X.

[33] H. Grasdalen, High-field, 1H-n.m.r. spectroscopy of alginate: sequential structure and linkage conformations, Carbohydrate Research. 118 (1983) 255–260. https://doi.org/10.1016/0008-6215(83)88053-7.

[34] Standard Test Method for Determining the Chemical Composition and Sequence in Alginate by Proton Nuclear Magnetic Resonance (1H NMR) Spectroscopy (Withdrawn 2021), (n.d.). https://www.astm.org/f2259-10r12e01.html (accessed April 15, 2021).

[35] K.I. Draget, G. Skjåk Bræk, O. Smidsrød, Alginic acid gels: the effect of alginate chemical composition and molecular weight, Carbohydrate Polymers. 25 (1994) 31–38. https://doi.org/10.1016/0144-8617(94)90159-7.

[36] D. Al Mahrouqi, J. Vinogradov, M.D. Jackson, Zeta potential of artificial and natural calcite in aqueous solution, Advances in Colloid and Interface Science. 240 (2017) 60–76. https://doi.org/10.1016/j.cis.2016.12.006.

[37] I. Langmuir, The adsorption of gases on plane surfaces of glass, mica and platinum., ACS Publications. (1918). https://doi.org/10.1021/ja02242a004.

[38] L.-M. Sun, F. Meunier, N. Brodu, M.-H. Manero, Adsorption Aspects théoriques, (2016). https://doi.org/10.51257/a-v2-j2730.

[39] D. Babayan, C. Chassenieux, F. Lafuma, L. Ventelon, J. Hernandez, Formation of Rodlike Silica Aggregates Directed by Adsorbed Thermoresponsive Polymer Chains, Langmuir. 26 (2010) 2279–2287. https://doi.org/10.1021/la902726f.

[40] H. Bessaies-Bey, J. Fusier, M. Hanafi, S. Zhang, M. Destarac, S. Jouenne, N. Passade-Boupat, F. Lequeux, J.-B. d'Espinose de Lacaillerie, N. Sanson, Competitive adsorption of PAM and HPAM on siliceous material, Colloids and Surfaces A: Physicochemical and Engineering Aspects. 579 (2019) 123673. https://doi.org/10.1016/j.colsurfa.2019.123673.

[41] V. Arumughan, T. Nypelö, M. Hasani, A. Larsson, Calcium Ion-Induced Structural Changes in Carboxymethylcellulose Solutions and Their Effects on Adsorption on Cellulose Surfaces, Biomacromolecules. 23 (2022) 47–56. https://doi.org/10.1021/acs.biomac.1c00895.

[42] K. Vermöhlen, H. Lewandowski, H.-D. Narres, M.J. Schwuger, Adsorption of polyelectrolytes onto oxides — the influence of ionic strength, molar mass, and Ca2+ ions, Colloids and Surfaces A: Physicochemical and Engineering Aspects. 163 (2000) 45–53. https://doi.org/10.1016/S0927-7757(99)00429-X.

[43] C.M. Ek, La dissolution du carbonate de calcium Essai de mise au point, BSGLg. (1973). https://popups.uliege.be/0770-7576/index.php?id=4983 (accessed May 10, 2021).

[44] A. Yan, Y. Xue, Z. Cui, Z. Zhang, S. Wang, Size-dependent dissolution kinetics of CaCO3 nanoparticles in theory and experiment, J Mater Sci. 52 (2017) 4412–4420. https://doi.org/10.1007/s10853-016-0688-8.

[45] B. Maciel, C. Oelschlaeger, N. Willenbacher, Chain flexibility and dynamics of alginate solutions in different solvents, Colloid Polym Sci. 298 (2020) 791–801. https://doi.org/10.1007/s00396-020-04612-9.

[46] I. Donati, S. Paoletti, Material Properties of Alginates, in: B.H.A. Rehm (Ed.), Alginates: Biology and Applications, Springer, Berlin, Heidelberg, 2009: pp. 1–53. https://doi.org/10.1007/978-3-540-92679-5_1.

[47] M. Thomas, J.A. Clouse, Thermal analysis of compounds adsorbed on low-surface-area solids. Part 1. Measurement and characterization by TGA., (n.d.).

[48] N.G. Hoogeveen, Adsorption of polyelectrolytes and charged block copolymers on oxides: consequences for colloidal stability, publisher not identified, Wageningen, 1996.

[49] G.J. Fleer, M.A.C. Stuart, J.M.H.M. Scheutjens, T. Cosgrove, B. Vincent, Polymers at Interfaces, Springer Netherlands, Dordrecht, 1998. https://doi.org/10.1007/978-94-011-2130-9.

[50] S. Stoll, P. Chodanowski, Polyelectrolyte Adsorption on an Oppositely Charged Spherical Particle. Chain Rigidity Effects, Macromolecules. 35 (2002) 9556–9562. https://doi.org/10.1021/ma020272h.

[51] S. Ulrich, A. Laguecir, S. Stoll, Complexation of a Weak Polyelectrolyte with a Charged Nanoparticle. Solution Properties and Polyelectrolyte Stiffness Influences, Macromolecules. 38 (2005) 8939–8949. https://doi.org/10.1021/ma051142m.

[52] X. Duan, M. Ding, R. Zhang, L. Li, T. Shi, L. An, Q. Huang, W.-S. Xu, Effects of Chain Rigidity on the Adsorption of a Polyelectrolyte Chain on Mixed Lipid Monolayer: A Monte Carlo Study, J. Phys. Chem. B. 119 (2015) 6041–6049. https://doi.org/10.1021/acs.jpcb.5b00515.

[53] E. Guzmán, F. Ortega, N. Baghdadli, G.S. Luengo, R.G. Rubio, Effect of the molecular structure on the adsorption of conditioning polyelectrolytes on solid substrates, Colloids and Surfaces A: Physicochemical and Engineering Aspects. 375 (2011) 209–218. https://doi.org/10.1016/j.colsurfa.2010.12.012.

[54] S. Llamas, E. Guzmán, F. Ortega, N. Baghdadli, C. Cazeneuve, R.G. Rubio, G.S. Luengo, Adsorption of polyelectrolytes and polyelectrolytes-surfactant mixtures at

surfaces: a physico-chemical approach to a cosmetic challenge, Advances in Colloid and Interface Science. 222 (2015) 461–487. https://doi.org/10.1016/j.cis.2014.05.007.

[55] S. Cao, L. Li, B. Zhu, Z. Yao, Alginate modifying enzymes: An updated comprehensive review of the mannuronan C5-epimerases, Algal Research. 69 (2023) 102952. https://doi.org/10.1016/j.algal.2022.102952.

Adsorption of sodium alginate on calcium carbonate microparticles: effect of molar mass and composition

R. Da Costa[a, b], C. Ghobril[b], P. Perrin[a,*], N. Sanson[a,*]

[a]Soft Matter Sciences and Engineering, PSL Research University, ESPCI Paris, Sorbonne Université, CNRS UMR 7615, 10 rue Vauquelin, 75231 Paris Cedex 05, France.
[b]L'Oréal Research & Innovation, Avenue Eugène Schueller 1, 93601 Aulnay-sous-Bois, France.

Supporting Information

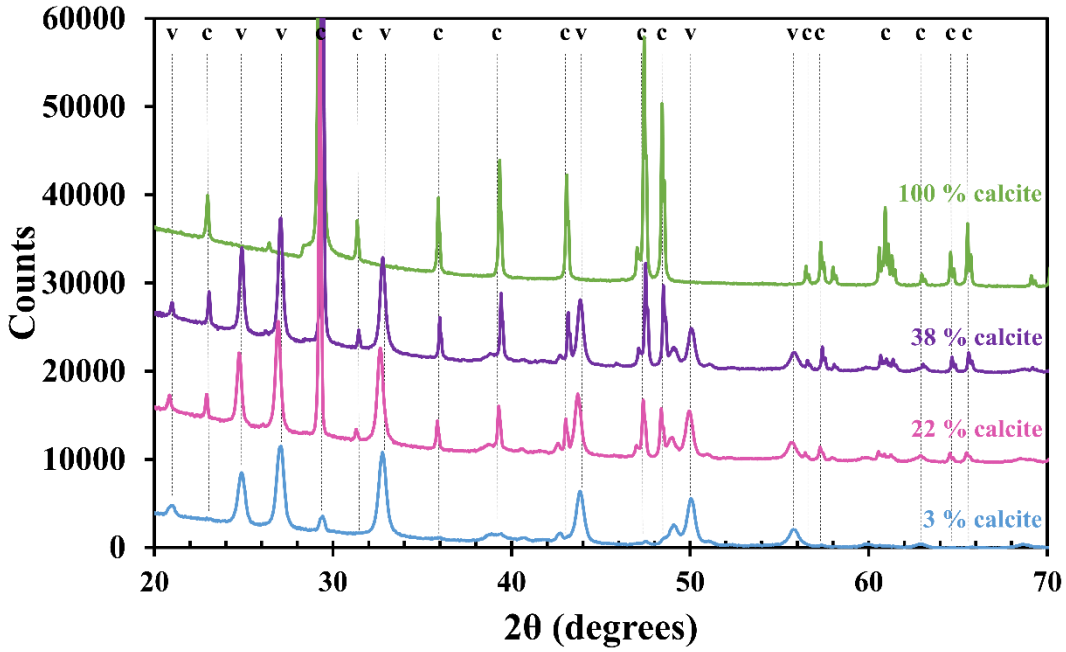

Fig. S1: XRD spectra of calcium carbonate ($CaCO_3$) microparticles studied in this article. Characteristic peaks of calcite (c) and vaterite (v) are identified.

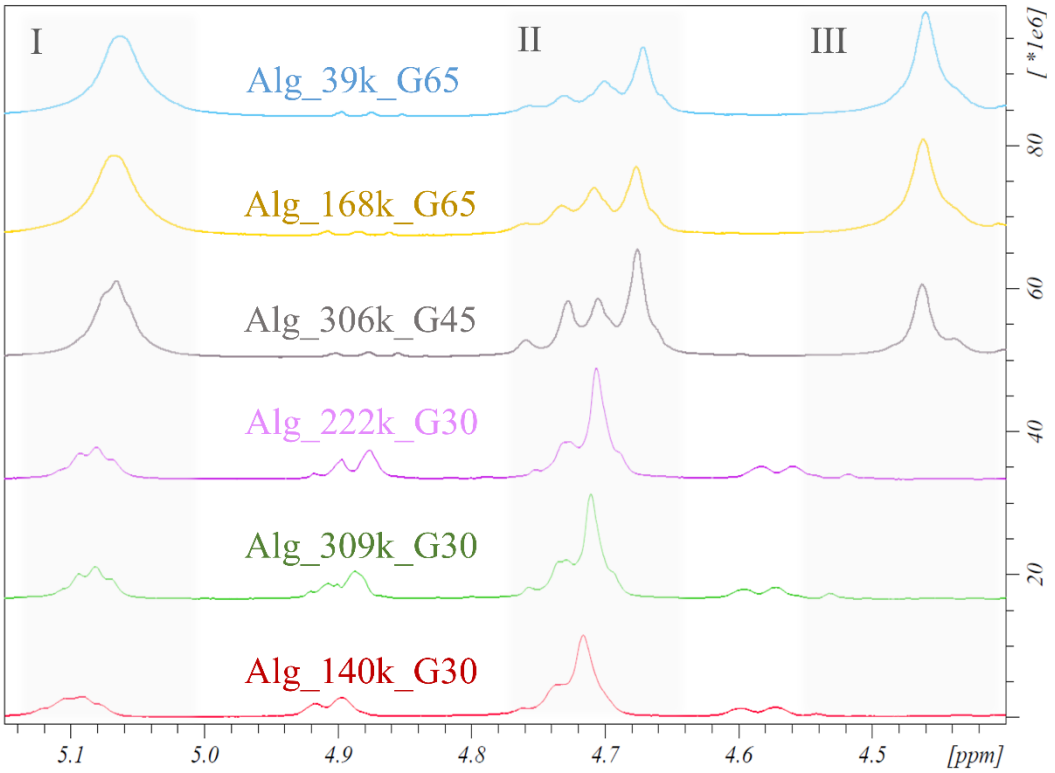

Fig. S2: ^{1}H-NMR spectra of mildly hydrolyzed sodium alginate (Na-Alg) performed at 80 °C with the different peaks of interest: I) 5.1-5.2 ppm, anomeric hydrogen of guluronic acid; II) 4.7-4.9 ppm, overlap of the anomeric hydrogen of mannuronic acid and of the H-5 of alternating MG-diblocks and, III) 4.5-4.6 ppm, H-5 of guluronic acid in G-blocks.

Table S1: Values of the theoretical adsorption model of Langmuir.

		Experimental data	Values from Langmuir equation		
$CaCO_3$	Na-Alg	Γ_{max} ($mg.m^{-2}$)	Γ_{max} ($mg.m^{-2}$)	r^2-fit	K_L ($L.mg^{-1}$)
$CaCO_3$_100%	Alg_306k_G45	0.90 ± 0.1	0.99	0.93	0.034
	Alg_309k_G30	1.60 ± 0.10	2.03	0.99	0.010
	Alg_222k_G30	1.5 ± 0.2	2.79	0.91	0.002
	Alg_140k_G30	N/A		N/A	
	Alg_168k_G65	9.3 ± 2.0	12.47	0.98	0.010
	Alg_39k_G65	11.5 ± 1.0	13.47	0.95	0.015
$CaCO_3$_38%	Alg_306k_G45	0.57 ± 0.1	0.62	0.93	0.030
	Alg_309k_G30	0.60 ± 0.1	0.66	0.94	0.025
	Alg_222k_G30	0.46 ± 0.07	0.63	0.91	0.006
	Alg_140k_G30	1.4 ± 0.2	1.71	0.96	0.011
	Alg_168k_G65	0.9 ± 0.4	0.76	0.54	0.027
	Alg_39k_G65	1.6 ± 0.5	1.37	1.00	0.035
$CaCO_3$_22%	Alg_309k_G30	0.40 ± 0.07	0.49	0.93	0.013
	Alg_140k_G30	1.18 ± 0.07	2.21	0.96	0.002

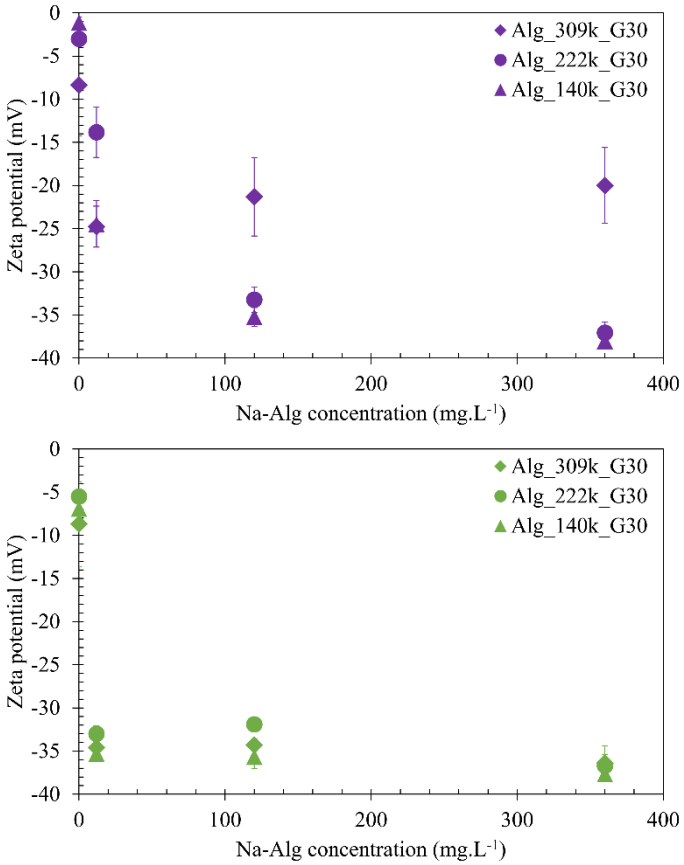

Fig. S3: Zeta potential of calcium carbonate ($CaCO_3$) microparticles ($CaCO_3$_100% in green and $CaCO_3$_38% in purple) after 4 hours in contact with aqueous solutions of sodium alginate (Na-Alg). Solid particles were dispersed in 10^{-3} mol.L^{-1} NaCl aqueous solutions at 20 °C before measurements.

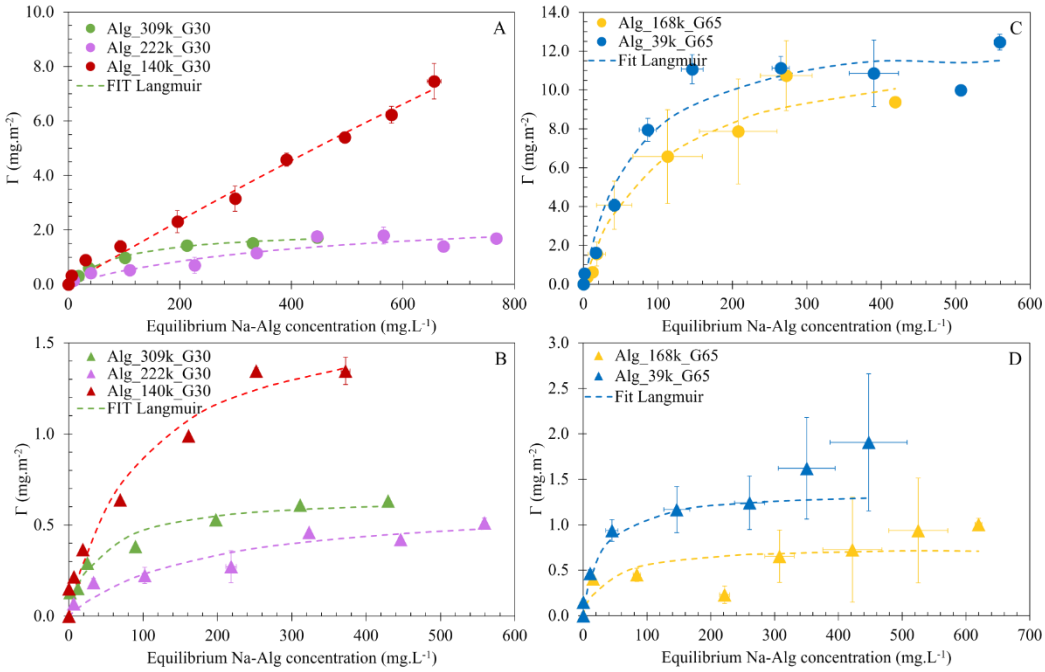

Fig. S4: Influence of sodium alginate (Na-Alg) average molar mass on their adsorption onto $CaCO_3$. A-D) adsorption isotherms of Na-Alg onto $CaCO_3$ microparticles. Red for Alg_140k_G30, green Alg_309k_G30, purple Alg_222k_G30, blue Alg_39k_G65 and yellow Alg_168k_G65. Rounds represent $CaCO_3$_100% (A and C) and triangles represent $CaCO_3$_38% (B and D). Lines represent the Langmuir isotherm fit.

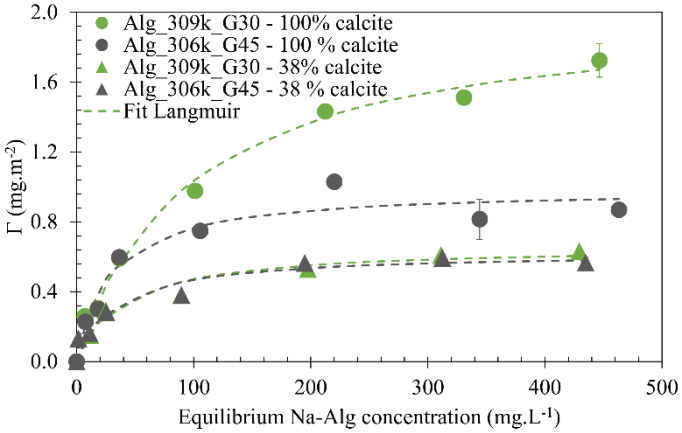

Fig. S5: Influence of the proportion of G-blocks in the backbone of Na-Alg with a molar mass of approximately 300 $kg.mol^{-1}$ on their adsorption onto $CaCO_3$. Adsorption isotherms of Na-Alg onto $CaCO_3$ microparticles: green Alg_309k_G30 and grey Alg_306k_G45. Rounds represent $CaCO_3$_100% and triangles represent $CaCO_3$_38%. Lines represent the Langmuir isotherm fit.